ACSNANO

www.acsnano.org

ARTICLE

Simultaneous Inhibition of Zn Dendrites and Polyiodide Ions Shuttle Effect by an Anion Concentrated Electrolyte Membrane for Long Lifespan Aqueous Zinc–Iodine Batteries

Pengxiang Lin, Guanhong Chen, Yuanhong Kang, Minghao Zhang, Jin Yang, Zeheng Lv, Yang Yang,* and Jinbao Zhao*

Cite This: *ACS Nano* 2023, 17, 15492–15503

Read Online

ACCESS | Metrics & More | Article Recommendations | Supporting Information

ABSTRACT: Aqueous zinc–iodine ($Zn–I_2$) batteries have attracted extensive attention due to their merits of inherent safety, wide natural abundance, and low cost. However, their application is seriously hindered by the irreversible capacity loss resulting from both anode and cathode. Herein, an anion concentrated electrolyte (ACE) membrane is designed to manipulate the Zn^{2+} ion flux on the zinc anode side and restrain the shuttle effect of polyiodide ions on the I_2 cathode side simultaneously to realize long-lifetime separator-free $Zn–I_2$ batteries. The ACE membrane with abundant sulfonic acid groups possesses a multifunctional amalgamation of good mechanical strength, guided Zn^{2+} ion transport, and effective charge repulsion of polyiodide ions. Moreover, rich ether oxygen, carbonyl, and S–O bonds in anionic polymer chains will form hydrogen bonds with water to reduce the proportion of free water in the ACE membrane, inhibiting the water-induced interfacial side reactions of the Zn metal anode. Besides, DFT calculations and *in-situ* UV–vis and *in situ* Raman results reveal that the shuttle effect of polyiodide ions is also significantly suppressed. Therefore, the ACE membrane enables a long lifespan of Zn anodes (3700 h) and excellent cycling stability of $Zn–I_2$ batteries (10000 cycles), thus establishing a substantial base for their practical applications.

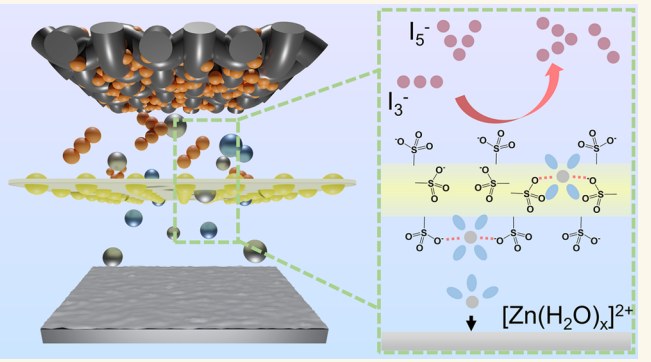

KEYWORDS: *aqueous zinc–iodine batteries, anion concentrated electrolyte membrane, guided Zn^{2+} ion flux, free water, polyiodide ions shuttle effect*

INTRODUCTION

Owing to the regional and intermittent obstacles of renewable energy, developing effective and high-safety electrochemical energy storage technologies for large-scale applications has become a major challenge for realizing carbon neutrality all over the world.[1−3] Among various emerging battery systems, aqueous zinc metal batteries (ZMBs) are considered to be one of the most competitive candidates due to the intrinsic safety performance based on the utilization of nonflammable aqueous media and low-cost and high energy density characteristics of Zn metal anodes.[4−8] To date, conventional cathode materials for ZMBs are mainly MnO_2,[9−12] V_2O_5,[13,14] and Prussian blue analogues[15,16] based on the intercalation/deintercalation mechanism of Zn^{2+} ions in a crystalline host, which suffers from the limited kinetics due to the high electrostatic interaction between Zn^{2+} ions with two charges and metal-oxide framework.[7,17] Alternatively, the halide I_2 cathode shows comparative superiority over its intercalation competitors due to the direct and highly reversible conversion reaction mechanism of the I^0/I^- redox couple.[18,19] Moreover, the sustainable and cost advantages of ZMBs is further magnified by introducing the wide abundance and eco-friendly I_2 to replace transition-metal oxides.[20−22]

In spite of the outstanding adaptability for large-scale energy storage, there are still significant concerns about the practical

Received: February 16, 2023
Accepted: July 17, 2023
Published: August 3, 2023

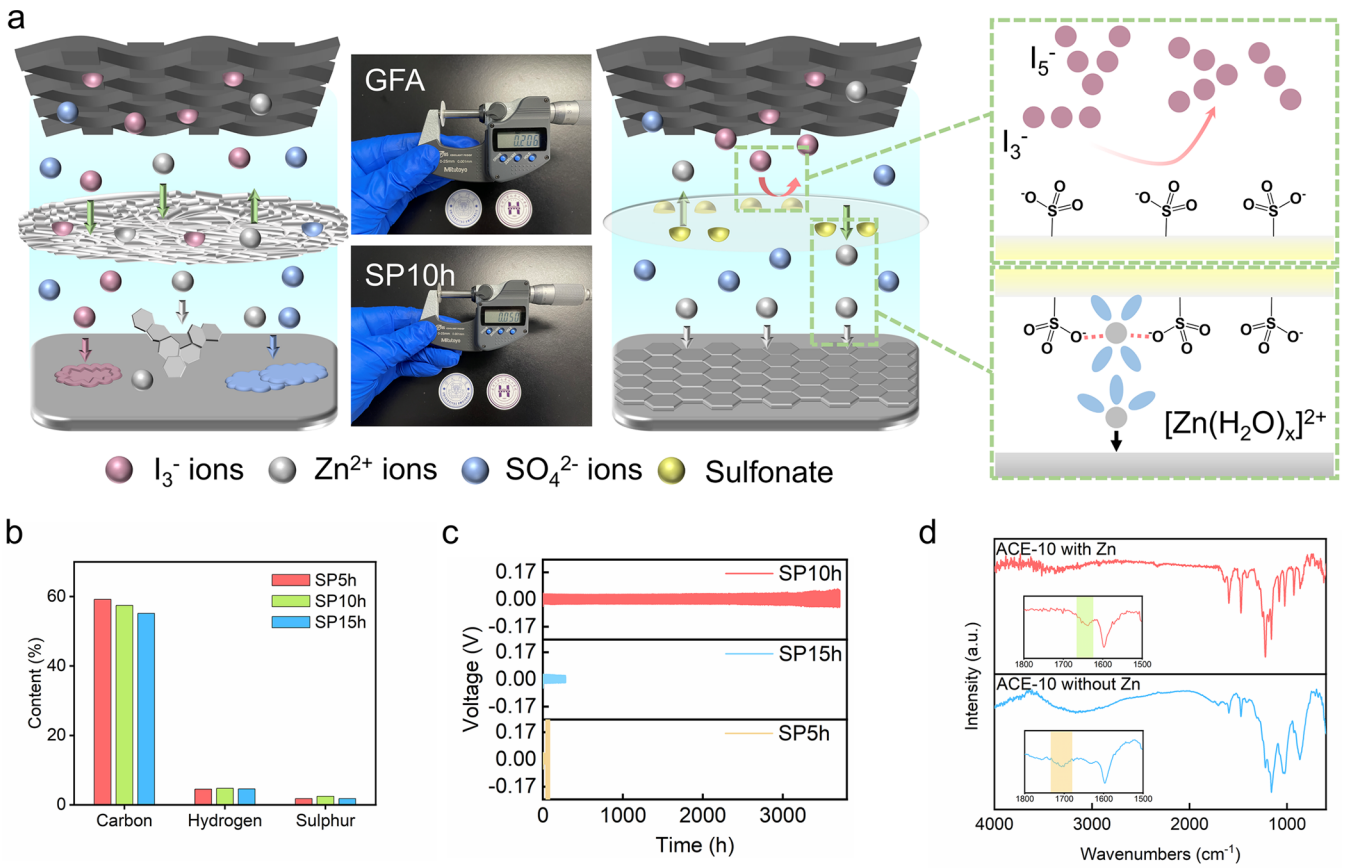

Figure 1. (a) Schematic diagram of the Zn−I_2 battery assembled with commercial GF/A separator and ACE-10 membrane and photos showing the thickness of these (all relevant badges are reviewed and approved by Xiamen University). (b) Elemental analysis of electrolytes with different sulfonation times. (c) Cycling comparison of Zn−Zn symmetric batteries of electrolytes with different sulfonation times. (d) Infrared spectrum of ACE-10 with or without Zn.

applications of Zn−I_2 batteries. On the Zn metal anode side, uncontrollable zinc dendrite growth and side reactions will lead to poor cycling stability and eventually internal short-circuit.[23,24] On the other hand, insoluble I_2 in the cathode tends to combine with I^- to form soluble polyiodide ions (I_3^- and I_5^- anions) into the electrolyte, leading to self-discharge and overcharge issues with unsatisfactory Coulombic efficiency.[22,25] More severely, the shuttle effect of intermediate polyiodide ions will react with anode materials, leading to the irreversible loss of cathode active materials and self-corrosion of Zn metal anodes, deteriorating the whole electrochemical performance of Zn−I_2 batteries dramatically.[22,26] Therefore, addressing these problems occurring in both the anode and cathode simultaneously is necessary for the development of high-performance Zn−I_2 batteries.

In response to these challenges, extensive efforts have been devoted, including the modification of the Zn anode and I_2 cathode, respectively. In terms of zinc anode optimization, surface modification,[27−29] host structure design,[30,31] and artificial SEI fabrication[32] are proposed to suppress the corrosion and dendrite growth. For the case of the I_2 cathode, confining I_2 into a porous conductive structure including porous carbon,[33] conducting polymers[34,35] and metal−organic frameworks[36] have been also extensively studied. However, the additional interfacial protective layer will inevitably increase the electrode weight and lower the battery energy density. Alternatively, the electrolyte regulation strategy, which does not need a specific electrode design, seems to be a more simple and efficient approach. From a fundamental view, both the issues of zinc anode passivation and shuttle effect are closely associated with the instable electrochemical interfaces.[25,37,38] Particularly, abundant free water molecules in the electrolyte will not only cause the corrosion and hydrogen evolution reactions of Zn metal, but also promote the I_2 cathode dissolution.[21,30] Therefore, various electrolyte designs have been proposed to modify the solvation structure, including high-concentration electrolytes,[39,40] functional electrolyte additives,[26,41,42] and deep eutectic electrolytes.[18] It should be noted that the realistic electrode/electrolyte environment in the battery configuration always involves the existence of a porous separator, and its effect of physical interruption on Zn plating and polyiodide ions transport also cannot be overlooked. Therefore, some pioneering studies have been also focused on well-designed functionalized separators to manipulate the interfacial chemistry.[43−45] Increasing evidence demonstrates that adjusting the thickness of the separator, introducing zincophilic functional groups, and controlling the pore size on the separator is beneficial for achieving flat dendrite-free zinc metal deposition.[45−49] Moreover, fabricating compact zeolite[50] and MOF separator[25,51] without micropores also shows good potential in suppressing the shuttle effect of polyiodide ions through the physical screening effect. Despite the impressive progress, most electrolyte or separator modification strategies still focus on the modification of individual Zn metal anode or I_2 cathode interfaces.[34,44,52] It is thus of great interest to achieve smooth Zn deposition

https://doi.org/10.1021/acsnano.3c01518
ACS Nano 2023, 17, 15492−15503

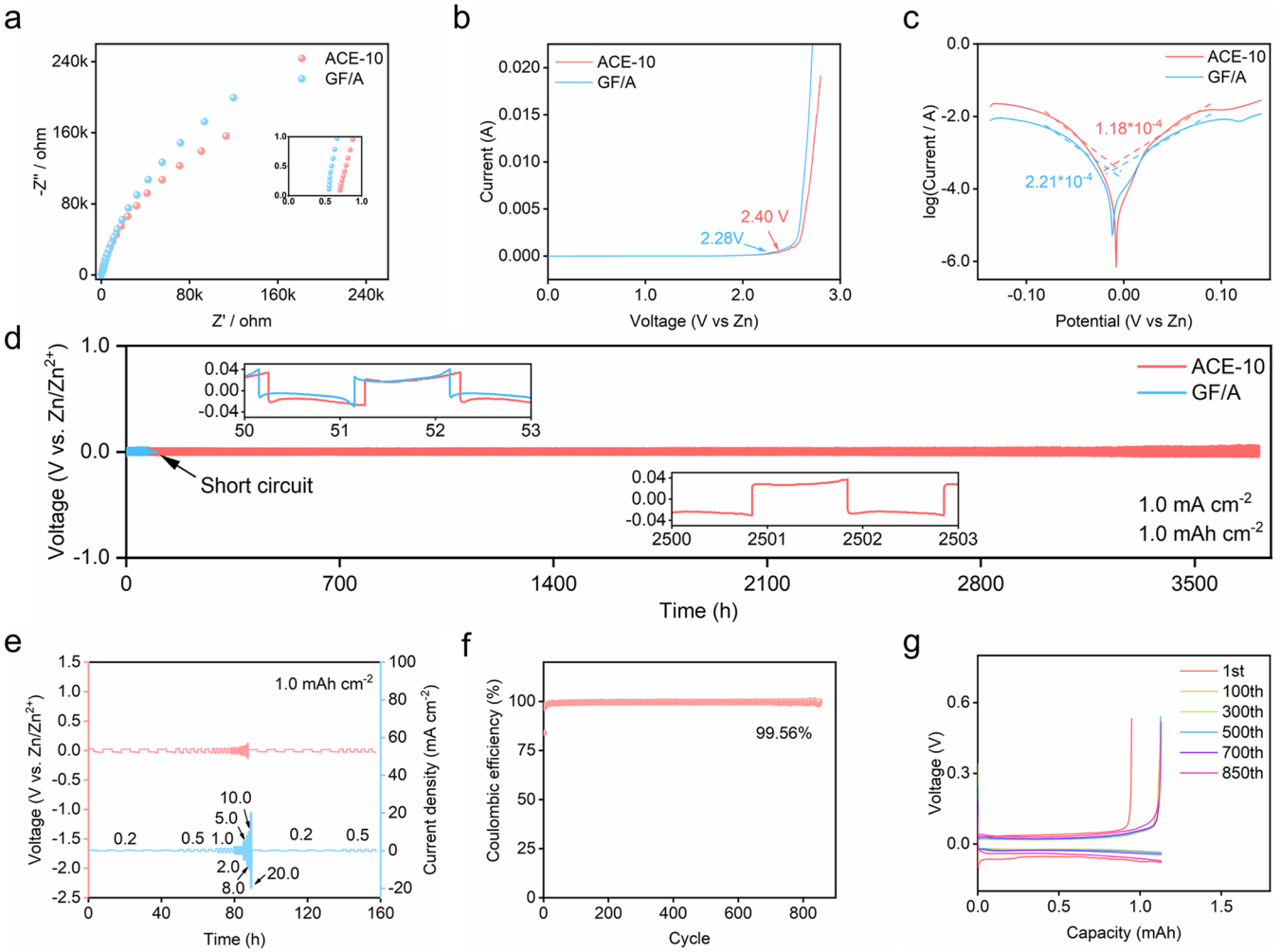

Figure 2. (a) Impedance spectra of GF/A and ACE-10 membrane (inset: the high frequency region). (b) Electrochemical window of ACE-10 membrane. (c) Tafel curves of electrolyte of GF/A and ACE-10 membrane. (d) Cycling curves of symmetric battery using diverse separators, the panels are 25th, 1250th cycles. (e) Cyclic voltage curves of Zn−Zn battery using ACE-10 membrane at different current densities. (f) Cycling performance of Zn−Cu half-battery assembled with ACE-10 membrane. (g) Capacity-voltage curves of Zn−Cu half cell using ACE-10 membrane.

behavior and restrain the shuttle effect of polyiodide ions simultaneously through a simple electrolyte/separator approach.

In this study, we demonstrate an anion concentrated electrolyte (ACE) membrane to manipulate the Zn^{2+} ion flux on the zinc anode side and inhibit the shuttle effect of polyiodide ions on the I_2 cathode side simultaneously to realize long lifespan Zn−I_2 batteries, which is enabled by constructing Zn^{2+}-coordinated sulfonated polyetheretherketone. The ACE membrane with abundant sulfonic acid groups possesses a multifunctional amalgamation of high mechanical strength, guided Zn^{2+} ion transport, and effective charge repulsion of polyiodide ions. Importantly, the ACE membrane contains an extremely low amount of water (53.4 wt%) compared with a conventional glass fiber separator in liquid electrolyte (931.5 wt%). Meanwhile, rich ether oxygen, carbonyl, and S−O bonds in anionic polymer chains will form hydrogen bonds with water to reduce the proportion of free water in the ACE membrane. As a result, the reduced water activity can not only inhibit the water-induced interfacial side reactions of Zn but also reduce I_2 dissolution of the positive electrode. Consequently, the separator-free Zn−I_2 battery using the ACE membrane exhibits an ultralong cycle life of 10000 cycles at 5 C.

RESULTS AND DISCUSSION

The functionalized electrolyte was prepared by a simple tape casting method and subsequent sulfonation treatment by using commercial PEEK powder as the starting material. (For synthesis details, please refer to Supporting Information.). As shown in Figure 1a and Figure S1, the synthesized ACE membrane (~50 μm) is significantly thinner than the commercial GF/A glass fiber separator (~206 μm), which is beneficial for improving the energy density of batteries. In order to explore the effect of different sulfonation times, ACE-5, ACE-10, and ACE-15 membranes are obtained by changing water bath sulfonation time as 5, 10, and 15 h, respectively (Figure S2). It can be seen from the XRD pattern (Figure S3) that the characteristic peaks of amorphous carbon are gradually weakened with the increase of the sulfonation time. This indicates that sulfonation treatment will also damage the polymer chain; thus, a longer sulfonation time may reduce the mechanical strength of electrolyte membrane. SEM images and EDS mapping of ACE-5, ACE-10, and ACE-15 membranes are

https://doi.org/10.1021/acsnano.3c01518
ACS Nano 2023, 17, 15492−15503

further obtained. As shown in Figure S4, the membranes sulfonated for different times all show relatively flat surfaces, and zinc ions are successfully exchanged into the electrolytes by soaking in 2.0 M $ZnSO_4$ solution. It can be seen in the high-resolution SEM images (Figure S5) that the surface of the electrolyte membrane becomes rougher with increasing sulfonation time. The contact angle test shows that the wettability of membranes to the electrolyte increased with the sulfonation time (Figure S6). In addition, it can be seen from the infrared spectrum that the electrolyte membrane shows obvious characteristic peaks of the sulfonic acid group, which indicates the successful introduction of sulfonic acid groups through a sulfonation reaction (Figure 1d). The above characterization results demonstrate that the sulfonation reaction not only introduces a sulfonate group to the benzene ring but also results in structural changes in the polymer chain. Therefore, determining an appropriate sulfonation reaction duration to achieve a balance between the degree of sulfonation and mechanical property is a key point for the high-performance ACE membrane.

In order to further explore the effect of sulfonation time on the membranes, we carried out elemental analysis tests on ACE-5, ACE-10, and ACE-15 membranes, respectively. The contents of H and S increased from ACE-5 to ACE-10 membranes, but unexpectedly decrease while further extending the reaction duration to 15 h, indicating that the content of the sulfonic acid groups on the membrane and the sulfonation time are not a simple linear relation (Figure 1b). Since a severe damage to the main chain will cause polymer degradation. Zn−Zn symmetric batteries using electrolyte membranes with various sulfonation times were shown in Figure 1c (1.0 mA cm^{-2} and 1.0 mAh cm^{-2}). It is found that the Zn−Zn symmetric battery assembled with an ACE-10 membrane sulfonated for 10 h delivers a cycle life over 3700 h. The batteries assembled with ACE-5 and ACE-15 membranes could only maintain stable cycling for about 20 and 300 h, respectively. Therefore, our subsequent experiments will be performed based on the ACE-10 membrane. The ACE-10 membrane contains an extremely low amount of water (53.4 wt%) compared with a conventional glass fiber separator in liquid electrolyte (931.5 wt%). After the ACE-10 membrane is completely dried, its porosity is determined to be only 0.41 mL g^{-1} by using a mercury porosimeter, which is much lower than that of commercial GF/A separator (Figure S7). Cross-sectional SEM images and EDS mapping of the ACE-10 membrane show very compact and uniform morphology without obvious cracks (Figure S8), implying that water in the ACE-10 membrane tends to be bound to polymer chains but does not exist in pores. Simultaneously, the red shift of the sulfonate group in the infrared spectrum (Figure 1d,1705 cm^{-1} to 1650 cm^{-1}) and the increase of the decomposition temperature of the sulfonate group in the thermogravimetric analysis (Figure S9, 295 to 383 °C) all indicate that Zn^{2+} ions were successfully exchanged into the ACE-10 membrane.[53−55] Besides, the tensile strength of commercial GF/A and the synthesized ACE-10 membrane are tested by a tensile tester (Figure S10), and the mechanical performance of the ACE-10 membrane far exceeded that of GF/A.

$$\sigma = F/s \quad (1)$$

The measured mechanical property of the ACE-10 membrane is superior than many recently reported hydrogel electrolytes and separators, but which still can not reach the high level of tensile strength for the nanocellulose-carboxymethylcellulose electrolyte.[56−63] These results suggest that the ACE-10 membrane has a good application prospect as an electrolyte for Zn−I_2 batteries.

Then, we explored the electrochemical performance of the ACE-10 membrane. As shown in Figure 2a, the electrochemical impedance spectra of GF/A (using 2 M zinc sulfate solution) and the synthesized ACE-10 membrane are tested respectively, and the ionic conductivity of ACE-10 membrane is calculated to be 13.46 mS cm^{-1}, which is only slightly lower compared to that of the aqueous electrolyte using the GF/A separator (31.65 mS cm^{-1}). The electrochemical window can reflect the applicable range of the electrolyte. As shown in Figure 2b, the LSV curve shows that the electrolyte exhibits a stable electrochemical window in the voltage range of ∼2.4 V, demonstrating that the electrolyte is compatible with conventional cathode materials for ZIBs. Tafel analysis is carried out using GF/A, ACE-10 membrane as electrolyte, and Zn foil as electrode to assemble Zn−Zn symmetric batteries. As shown in Figure 2c, the corrosion current of the symmetric battery assembled with the ACE-10 membrane is 1.04×10^{-4} mA cm^{-2}, while that of the GF/A-assembled symmetric battery is 1.96×10^{-4} mA cm^{-2}. This indicates that the ACE-10 membrane can also inhibit the corrosion of the zinc foil by reducing the proportion of free water.

To evaluate the durability of the ACE-10 membrane, we assembled and tested Zn−Zn symmetric batteries. As shown in Figure 2d, the Zn−Zn symmetric battery using the GF/A separator can only be cycled for ∼150 h before the short circuit at 1.0 mA cm^{-2} with a plating/stripping capacity of 1.0 mAh cm^{-2}. However, the Zn−Zn symmetric battery assembled with the synthesized ACE-10 membrane can be cycled stably for more than 3700 h. The Zn//Zn+ ACE-10 symmetric battery assembled at 2.0 mA cm^{-2}, 2.0 mAh cm^{-2} and 5.0 mA cm^{-2}, 5.0 mAh cm^{-2} can be cycled durably for over 600 h and close to 300 h, respectively (Figure S11). There is indeed an increase in cell polarization voltage at a current density of 2.0 mA cm^{-2} after 450 h, which may be associated with the contact environment revolution between the gel-type electrolyte and the zinc foil during repeated cycling.[45,64−66] The symmetric battery assembled with the ACE-10 membrane can retain stable cycling in the current density ranges of 0.2−10.0 mA cm^{-2} (Figure 2e), exhibiting good high-rate cycling endurance. Electrochemical reversibility is also an important indicator for metal anodes. Herein, the Zn//Cu+ACE-10 half cells were fabricated to evaluate the Coulombic efficiency. The half-battery using the ACE-10 membrane can be cycled stably for more than 800 cycles with an average Coulombic efficiency of 99.56% (Figure 2f) at 1.0 mA cm^{-2} with a capacity of 1.0 mAh cm^{-2}. The voltage-capacity profiles after different cycles show that the Zn−Cu half cell assembled with the ACE-10 membrane exhibits a very low overpotential, ensuring the relatively small electrochemical polarization of about 45 mV (Figure 2g). These illustrate that the synthesized ACE-10 membrane can effectively suppress the by-reaction arising from the Zn deposition/exfoliation process. Similarly, the CV test shows that the zinc deposition overpotential of the battery assembled with ACE-10 membrane is smaller, which indicates that the ACE-10 membrane renders Zn easier to be deposited (Figure S12).

To clarify the mechanism underlying the enhanced cycling stability of the Zn anodes, various characterizations were conducted. As shown in Figure 3a, the deposition morphology

https://doi.org/10.1021/acsnano.3c01518
ACS Nano 2023, 17, 15492−15503

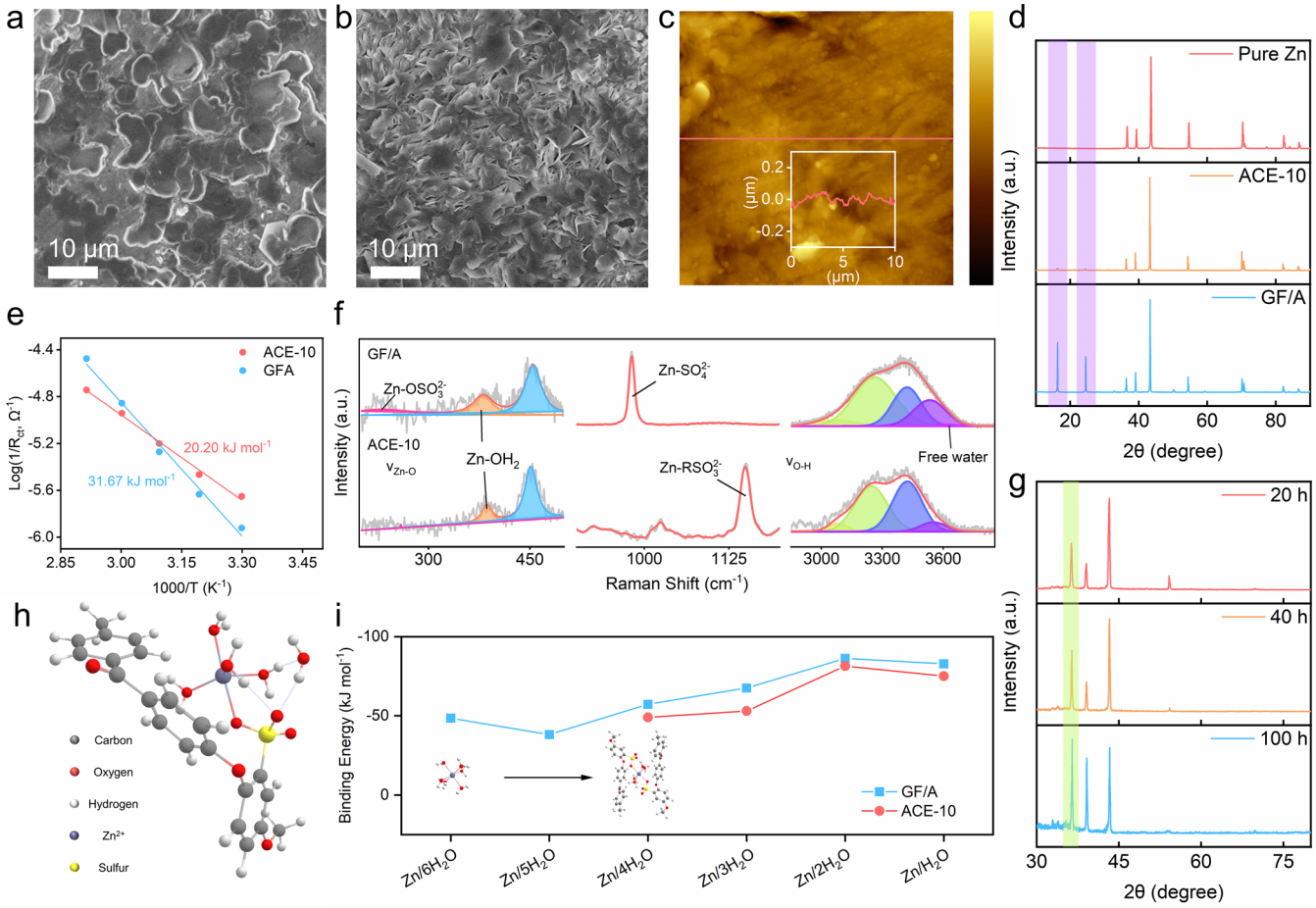

Figure 3. SEM images of Zn foils after 100 h cycling at 1.0 mA cm^{-2} for 1.0 mAh cm^{-2} in Zn−Zn symmetric batteries assembled with (a) ACE-10 membrane, (b) GF/A separator. (c) AFM images of the Zn foils after 100 h cycling at 1.0 mA cm^{-2} for 1.0 mAh cm^{-2} in Zn−Zn symmetric batteries assembled with ACE-10 membrane, the inset is a schematic diagram of the height change of the red line. (d) XRD patterns of the pristine Zn foil and Zn foils after 100 h cycling in symmetrical batteries with different electrolytes. (e) The desolvation activation energies of the two electrolytes calculated by the Arrhenius equation. (f) Raman spectroscopy of GF/A membrane (with 2.0 M $ZnSO_4$) and ACE-10 membrane including Zn−O stretch bond, ν-SO_4^{2-}, ν-RSO_3^{2-} band, and O−H stretch vibration. (g) Grazing-incidence XRD patterns of Zn foils after different cycles in symmetric batteries assembled with ACE-10 membrane. (h) Binding forms of zinc pentahydrate ions and ACE-10 membrane molecules obtained by computational simulation. (i) The binding energies of zinc ions hydrated with different amounts of water molecules in different electrolytes by calculation.

of Zn with ACE-10 membrane after cycling is relatively flat and smooth. By comparison, rampant dendrites and a lot of byproducts appeared on the surface of zinc foil with the GF/A separator (Figure 3b). To further illustrate that the ACE-10 membrane is beneficial for the flattening of zinc deposition, AFM images of zinc foils cycling with the two electrolytes respectively are obtained. As shown in Figure 3c, after 100 h of cycling, the surface of the zinc foil cycling with the ACE-10 membrane shows no obvious fluctuations. While the height difference of the zinc foil surface after cycling with the GF/A separator is dramatic (Figure S13). Besides, similar results can be obtained from the imaging of the laser shape measurement microscope (Figure S14, Table S1). The flatness of Zn foil surface after cycling with the ACE-10 membrane is significantly better than that with the GF/A separator.

In order to discuss the failure mechanism of the Zn−Zn symmetric battery, Zn foils after 100 h cycling in symmetric cells are taken out of the zinc foil for the XRD test. As shown in Figure 3d, comparing with the pristine zinc foil, obvious characteristic peaks of the byproduct [zinc sulfate hydroxide hydrate, $Zn_4(OH)_6SO_4{\cdot}5H_2O$, JCPDS No. 39-0688, the purple highlight] appear for the zinc foil cycling with the GF/A separator. On the contrary, the Zn foils cycling with the ACE-10 membrane show no obvious diffraction peaks. This means that the ACE-10 membrane can suppress the formation of byproducts effectively during the cycling process, which is related to the rich sulfonic acid groups on its surface. To eliminate the influence of the zinc substrate, GIXRD is used to characterize the crystal structure of deposited zinc. As shown in Figure 3g, the peak area of the (002) plane increases continuously with the passage of cycle time (highlighted in green). This indicates that the sulfonic acid groups on the ACE-10 membrane can make the zinc ions tend to deposit along the (002) plane during deposition. To prove that the guided preferential deposition direction of Zn ions is the role of the sulfonic acid groups on the ACE-10 membrane, we conducted a control experiment with a GF/A separator. As presented in Figure S15, there is no fixed changes of regularity for the crystal plane of deposited zinc. It further demonstrates that our synthesized ACE-10 membrane rich in sulfonic acid groups can guide the preferential orientation deposition of Zn ions.

https://doi.org/10.1021/acsnano.3c01518
ACS Nano 2023, 17, 15492−15503

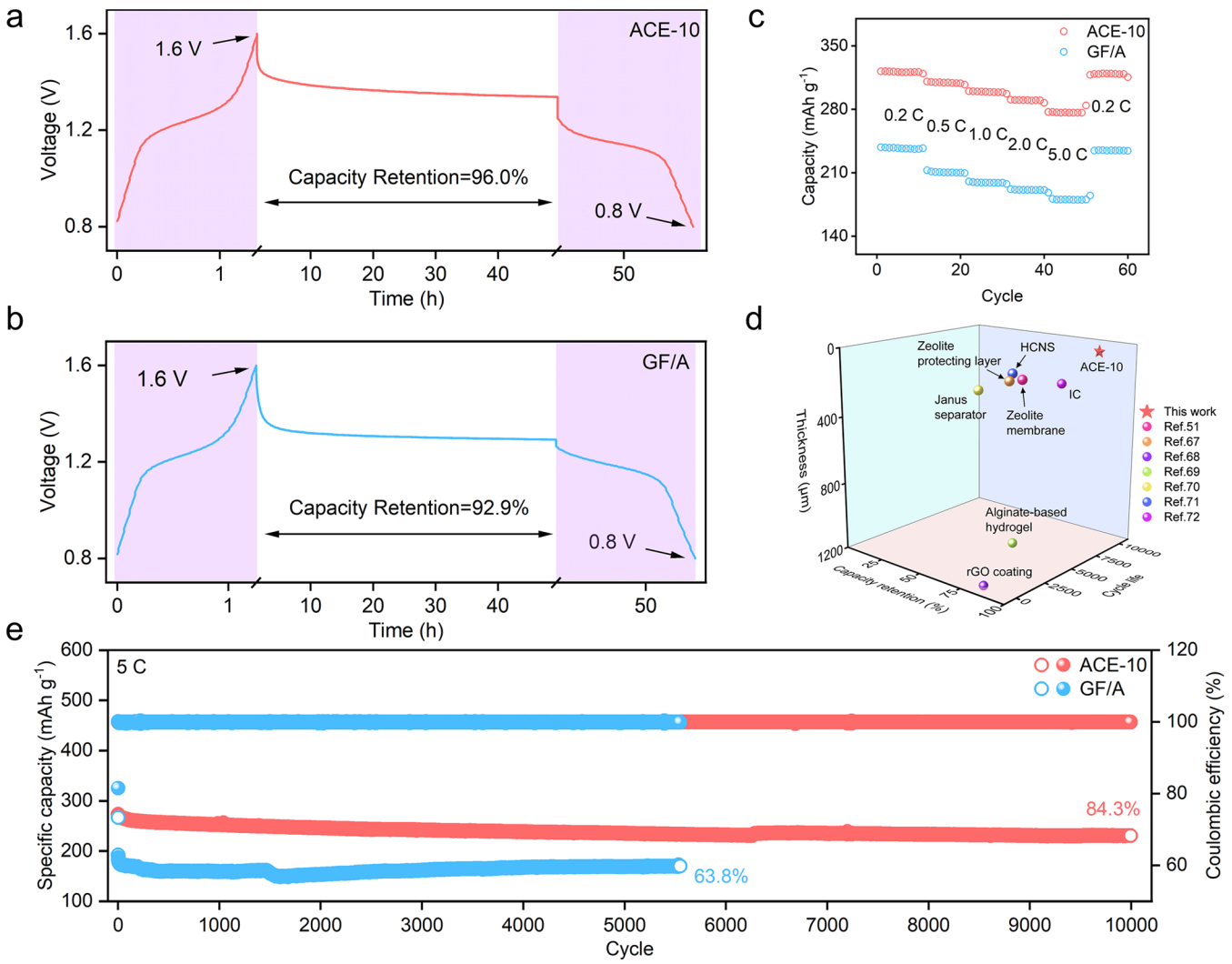

Figure 4. Assembled Zn−I_2 battery is charged to 1.6 V and then discharged to 0.8 V after shelving for 48 h, with (a) ACE-10 membrane and (b) GF/A as separator. (c) Rate performance of Zn−I_2 batteries assembled with ACE-10 and GF/A. (d) The comparison of electrochemical performance between the ACE-10 electrolyte and recently reported modified electrolytes for Zn−I_2 batteries. (e) Cycling performance of Zn−I_2 batteries with ACE-10 and GF/A at 5 C.

As mentioned earlier, the surface of Zn foil after cycling with commercialized GF/A separator exhibits severe accumulation of byproducts. This is because the solvated zinc ions have a strong configuration with the surrounding solvated sheath water molecules. The solvated zinc ions require enormous energy to remove the solvated sheath before the reduction of Zn^{2+} on the surface of the zinc electrode. These energies make HER and the followed generation of byproducts more prone to occur on the surface of Zn foil:[27,64,67]

$$4Zn^{2+} + 6OH^- + SO_4^{2-} + 5H_2O \rightarrow Zn_4(OH_6)SO_4{\cdot}5H_2O \quad (2)$$

Therefore, if the amount of water molecules in the solvation sheath can be reduced in advance, the generation of byproducts during deposition can be effectively suppressed. The activation energy is expressed by E_a in the Arrhenius equation as follows:[67,68]

$$k = A\, e^{-E_a/(RT)} \quad (3)$$

$$k = 1/R_{ct} \quad (4)$$

(A, frequency factor; R, gas constant; T, absolute temperature; R_{ct}, interface resistance).

To investigate the desolvation ability of the ACE-10 membrane, the variable temperature EIS impedance test method was used for the study. Figures S16 and S17 show that the R_{ct} of Zn foil with ACE-10 membrane (284.55 Ω) is smaller than that with GF/A separator (373.12 Ω) at 313.15 K (Table S2), implying the enhanced charge-transfer kinetics. Results shown in Figure 3e are obtained by fitting the Arrhenius equation. The activation energy E_a in the ACE-10 membrane is about 20.20 kJ mol^{-1}, while that in the GF/A membrane is about 31.67 kJ mol^{-1}, suggesting that the rich sulfonic acid groups in the ACE-10 membrane have a positive desolvation effect on hydrated zinc ions.

To explain the difference in desolvation properties theoretically, we simplified the superlong polymer chain of ACE-10 membrane into the structure of a single monomer. Computational simulations of this simplified structure with zinc ions show that the binding energy of sulfonic acid groups to zinc ions is moderate (Figures S18 and S19), which indicates that the surrounding Zn^{2+} ions are easy to be combined with sulfonic acid groups. From the chronoamper-

https://doi.org/10.1021/acsnano.3c01518
ACS Nano 2023, 17, 15492−15503

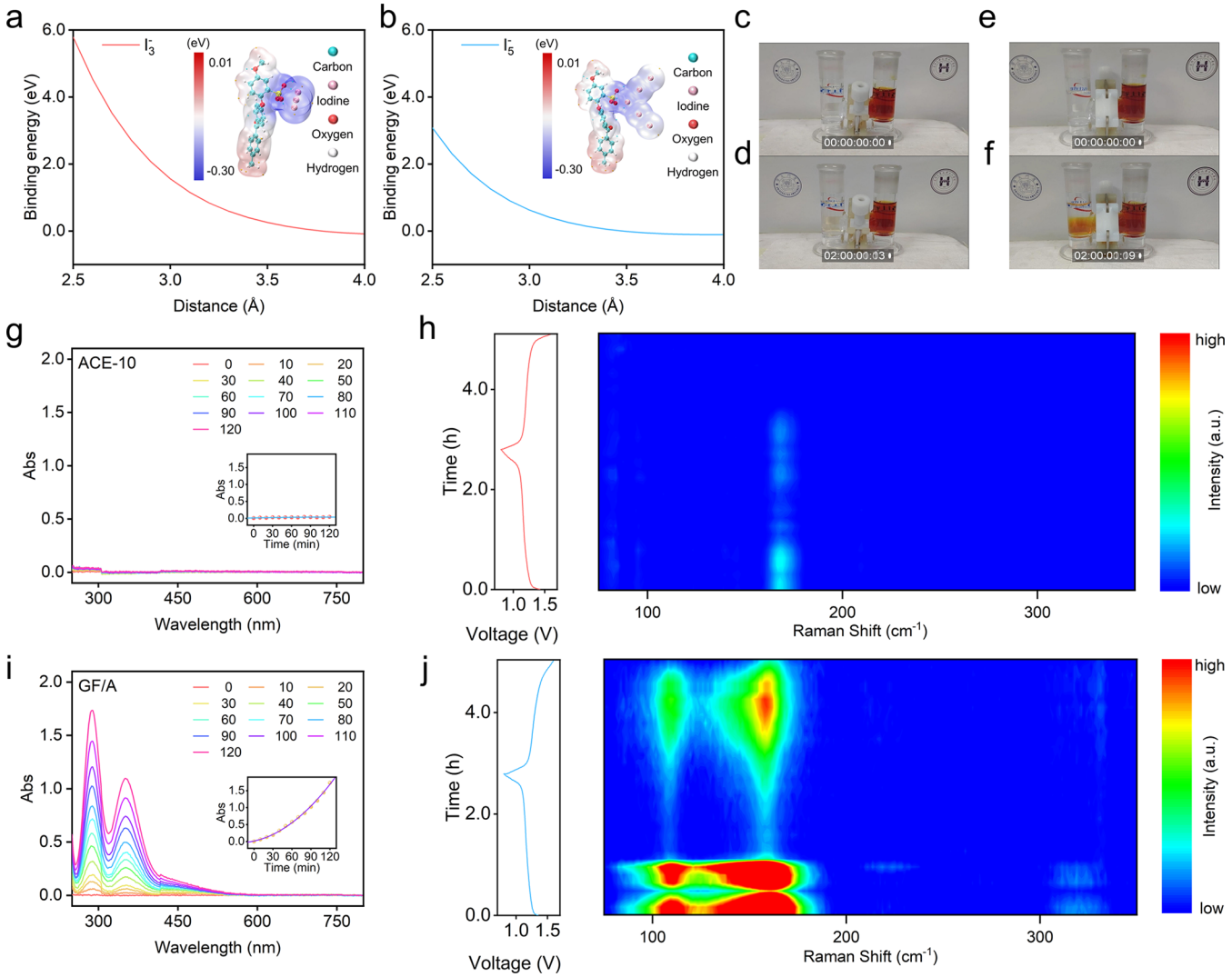

Figure 5. Electrostatic surface potential of ACE-10 with (a) I_3^- and (b) I_5^- ions. The shuttle effect of polyiodide ions observed by H-type electrolytic cell, where (c, d) ACE-10 and (e, f) GF/A are selected as electrolyte (all relevant badges are reviewed and approved by Xiamen University). UV−vis absorption spectra of the solution on the left side of the H-type electrolytic cell at different times, where (g) ACE-10, (i) GF/A are selected as electrolyte, respectively, and the inset is the fitting curve of the UV−vis absorption peak intensity at 178 nm versus time. *In-situ* Raman of Zn−I_2 batteries assembled with (h) ACE-10 membrane and (j) GF/A as electrolytes.

ometry at a constant overpotential of 10 mV, it was found that the current in the GF/A membrane decreased rapidly for 4000 s (Figure S20b), indicating that the planar diffusion and deposition processes are rampant. On the contrary, the behaviors of nucleation and diffusion in the ACE-10 membrane are completed in a shorter time, the curve changes slowly and finally becomes almost horizontal in the subsequent time (Figure S20a), which indicates that the zinc deposition is relatively dense.[69] Through ion chromatography and the ICP test (Figure S21), the ACE-10 membrane only contains a trace amount of SO_4^{2-} ions, while the content of Zn^{2+} is about 2.11 × 10^{-5} mol. The same can be obtained from the Raman spectrum (Figure 3f). Compared with the GF/A separator ACE-10 membrane, the peak intensity of Zn-OSO_3^{2-} (260 cm^{-1}, 981 cm^{-1}) is significantly reduced. The characteristic peak of Zn-RSO_3^{2-} appears at 1150 cm^{-1} in the ACE-10 membrane (as shown in Figure S22, the Zn-RSO_3^{2-} characteristic peak appears at 1088 cm^{-1} in $Zn(OTf)_2$; considering that the three fluorine atoms are a super strong electron-withdrawing group, the characteristic peak of zinc benzenesulfonate should be blue-shifted). Besides, it can be found from the peak of ν-OH that there is almost no free water (3650 cm^{-1}) in the ACE-10 membrane.[70−72] Through simulation calculations, it can be concluded that the carbonyl and ether on the molecular chain of the ACE-10 membrane can effectively immobilize water molecules in the electrolyte (Figure S23), reducing the activity of free water. These all indicates that the ACE-10 membrane can effectively reduce the effect of SO_4^{2-} ions and free water on the corrosion of zinc foil.

Finally, we define the desolvation energy by calculating the binding energies between the hydrated zinc ions and water molecules in a simplified molecular chain model. As shown in Figure 3i and Table S3, the sulfonic acid groups on the molecular chain can effectively reduce the desolvation energy during deposition, which is consistent with the previous experimental results. In the simulation, it was found that a simplified molecular chain (when there is only one sulfonic acid group) could not be stabilized when the zinc ions hydrated with five waters (Figure 3h), and one of the water molecules would break away from the coordination constraints

https://doi.org/10.1021/acsnano.3c01518
ACS Nano 2023, 17, 15492−15503

of Zn^{2+}, which is similar to the previous report.[73] Through further calculations, as shown in Figure S24 and Video S1, when the hexahydrated zinc ion is close to the ACE-10 molecule, two of the water molecules will move away (H_2O-1: 2.1933 to 2.4679 Å; H_2O-2: 2.2057 to 2.2102 Å). This further validates our previous conclusions.

As mentioned above, an ACE-10 membrane rich in sulfonic acid groups can be used as an electrolyte for zinc−iodine batteries because the sulfonic acid groups can effectively inhibit the shuttle effect of the polyiodide ions.[74,75] Therefore, ACC/I_2 is selected as the positive electrode material of the Zn−I_2 full batteries. As shown in Figure S25, when I_2 is adsorbed on ACC, the XRD characteristic peak intensity of the amorphous carbon decreases. In SEM and mapping (Figure S26), it can be clearly seen that I_2 is adsorbed on the surface of ACC. We first assembled the Zn−I_2 full batteries with ACE-10 membrane and GF/A as electrolytes, respectively, and all of the full batteries are activated for one cycle and then shelved for 48 h before discharging (Figure 4a,b). It can be seen from Figure 4a that the open circuit voltage of Zn//I_2 + GF/A dropped to 1.33 V in 6 h after activation, while the open circuit voltage of Zn//I_2 + ACE-10 only dropped to 1.40 V. Discharged at a current density of 1 C after 48 h of shelving, Zn//I_2+ACE-10 can deliver a capacity of 273.0 mAh g^{-1} (capacity retention rate is 96%), while Zn/GF/A/I_2 can only deliver an inferior capacity of 256.7 mAh g^{-1} (capacity retention rate is 92.9%, Figure S27). It shows that the ACE-10 membrane can effectively prevent the shuttle effect of the polyiodide ions, thus ensuring the capacity retention of the Zn−I_2 battery.

It can be seen from Figures 4c and S28 that the rate performance of Zn//I_2+ACE-10 is also significantly better than Zn//I_2+GF/A. To compare the long-cycle performance of Zn−I_2 full batteries, our assembled batteries were cycled at current densities of 1, 2, and 5 C, respectively. As shown in Figure S29, Zn//I_2 + ACE-10 can be stably cycled for over 1400 cycles at a current density of 1 C with a capacity retention rate as high as 88.5%, while Zn//I_2 + GF/A can only be cycled for less than 800 cycles. Besides, Zn//I_2 + ACE-10 is able to be cycled steadily for over 2500 cycles at a current density of 2 C with a capacity retention rate as high as 86.0% (Figure S30). The capacity retention rate of Zn//I_2 + GF/A is only 63.0%. The ACE-10 membrane battery could cycle stably for 10000 cycles at the current density of 5 C, with a capacity retention rate as high as 84.8%, while the GF/A battery is only 63.8% (Figure 4e and Figure S31). All of these indicate that our synthesized ACE-10 membrane is suitable for application in Zn−I_2 batteries. To have a better understanding on ACE-10 membrane battery, some representative electrolyte materials are compared on cycle life, thickness, and capacity retention (Figure 4d and Table S4).[50,76−81] Considering the importance of reducing the N/P ratio for practical battery application, Zn//I_2 + ACE-10 full batteries using a 30 μm thickness of zinc foil were also assembled. As shown in Figure S32, the batteries can also maintain stable cycling over 800 cycles at a current density of 5 C, with a capacity retention rate of 80.40%. This shows that the Zn−I_2 battery assembled with an ACE-10 membrane ensures a good electrochemical performance even under a limited amount of negative electrode.

In order to clarify the inhibition effect of the ACE-10 membrane on the shuttle of polyiodide ions, a simplified molecular chain model of the ACE-10 membrane with I_3^- and I_5^- ions is constructed through theoretical calculations, respectively. As shown in Figure 5a and b, both of the interaction energies between the sulfonic acid groups in the ACE-10 membrane and I_3^- or I_5^- ions are positive, verifying that the approach of I_3^- and I_5^- anions to polymer chains is energy-consuming, which should tend to be far from the electrolyte membrane surface. Therefore, the sulfonic acid groups on the molecular chain of ACE-10 membrane can repel I_3^- and I_5^- ions through the electrostatic interaction; thus, the shuttle effect of polyiodide ions during cycling is greatly impeded by the ACE-10 membrane. Moreover, the surface zeta potential of the ACE-10 membrane is also determined to be negative through the solid surface zeta potential test (Figure S33), further corroborating the DFT calculation results.

To further validate the charge repulsion of the ACE-10 membrane predicted by the theoretical calculations, the permeation of polyiodide ions is evaluated in the H-type electrolytic cell. Deionized water and 0.02 M polyiodide ion solution are added on either side. After 2 h, the solution on the left side of the ACE-10 membrane shows almost no color change (Figure 5c and d, Video S2), while the solution on the left side of the GF/A membrane has turned orange-red (Figure 5e,f, Video S3) (all relevant badges are reviewed and approved by Xiamen University). Meanwhile, the solutions on the left tubes are also taken out at the same time interval for UV−vis absorption spectroscopy to determine the content of the polyiodide ions in the solution. As shown in Figure 5g,i, the UV−vis absorption peak intensity of polyiodide ions in the ACE-10 membrane group hardly changed during 120 min, while the absorption peak intensity with the GF/A increased significantly. It indicates that the ACE-10 membrane can effectively inhibit the shuttle effect of polyiodide ions. Furthermore, *in situ* Raman tests were performed to further confirm whether the ACE-10 membrane can still take effect during battery cycling (current density: 0.5 C). As shown in Figure 5h and Figure S34, the ACE-10 membrane can suppress the shuttle effect of polyiodide ions during the initial charge/discharge cycle, and only a few characteristic peaks of I_5^- ions appear during the charging process. On the contrary, the electrolyte of Zn//I_2 + GF/A shows high-intensity characteristic peaks of I_3^- and I_5^- ions at the initial stage of battery discharge and charging (Figure 5j and Figure S35). Therefore, in comparison with the ACE-10 membrane, the GF/A separator whith high porosity cannot effectively suppress the shuttle effect of polyiodide ions during cycling of the Zn−I_2 battery.

CONCLUSION

In conclusion, we successfully prepared an anion concentrated electrolyte membrane with an ionic conductivity of 13.46 mS cm^{-1} through a simple sulfonation reaction. Theoretical calculations and experimental results show that the rich sulfonic acid groups in the electrolyte can bind with hydrated zinc ions, thereby effectively reducing the desolvation energy and ensuring orderly deposition of zinc ions. The assembled Zn−Zn symmetric batteries can be cycled steadily for more than 3700 h at 1.0 mA cm^{-2} for 1.0 mAh cm^{-2}, and the Zn−Cu half cell can be cycled for more than 800 cycles. *In-situ* Raman spectroscopy and other characterization methods indicate that the characteristics of rich sulfonic acid groups and no pores in the ACE-10 membrane can effectively suppress the shuttle effect of polyiodide ions. The assembled Zn//I_2 + ACE-10 battery shows high reversibility, excellent cycling durability, and an impressive rate capability. It is believed that demonstrating these properties of the ACE-10

https://doi.org/10.1021/acsnano.3c01518
ACS Nano 2023, 17, 15492−15503

membrane can provide inspiration in future work, thus promoting Zn−I_2 batteries to be more widely used.

METHODS

Synthesis of ACE-10 Membrane. 2.0 g of PEEK was put it into a three-necked flask, then 50 mL of 98% concentrated sulfuric acid is added, and the mixture is stirred for 10 h under 50 °C water bath. After dissolved completely, an orange-yellow viscous liquid is obtained. The solution is poured into ∼1 L of ice water. After the yellow liquid is completely converted into a pink solid, suction filtration is performed. The filter cake is washed three times with distilled water and dried in a vacuum oven to obtain the sulfonated SPEEK. For the preparation of ACE membrane, 0.75 g of SPEEK is dissolved in 10 mL of DMF, and the solution is transfered into a polytetrafluoroethylene mold, and placed on a hot plate at 60 °C for 6 h, and further dried in a vacuum oven at 100 °C for 12 h. The dried membrane is peeled off and soaked in ultrapure water for 24 h.[82,83] After that, it is placed in a 2.0 M $ZnSO_4$ solution for 48 h for zinc ion replacement (the solution needs to be replaced when the pH is lower than 4 during the period), and finally, the ACE-10 after ion replacement is obtained. The ACE-10 membrane needs to be stored in 2.0 M $ZnSO_4$ solution before using.

Synthesis of I_2 Cathode. I_2 cathodes are made through a sublimation diffusion method.[84,85] First, the ACC is treated with dilute HCl. Next, I_2 and ACC are mixed with a mass ratio of 1:2 in a sealed glassy reactor and then heated to 80 °C for 30 min. The real loading mass of iodine active material is obtained by subtracting the mass of ACC and I_2/ACC.

ASSOCIATED CONTENT

Supporting Information

The Supporting Information is available free of charge at https://pubs.acs.org/doi/10.1021/acsnano.3c01518.

Experimental details for the materials used in the experiment, characterizations, electrochemical measurements, LSV test method, CV test method, liquid absorption test method, binding energy calculation method, and desolvation energy calculation method, thickness comparison of ACE-10 membrane and GF/A separator, optical photographs of ACE-5, ACE-10, and ACE-15 membranes, XRD patterns of PEEK and ACE-5, ACE-10, ACE-15 membranes, SEM imaging and mapping of ACE-5, ACE-10, and ACE-15 membranes, High-resolution SEM images, contact angle measurements, comparison of total pore volume of commercial GF/A pore separators and ACE-10 membrane, sectional SEM imaging and mapping of ACE-10 membrane, thermogravimetric analysis of ACE-10 with Zn and ACE-10 without Zn, comparison of tensile strength between ACE-10 membrane and GF/A separator, cycle time-voltage curves of Zn//Zn+ACE-10 symmetric batteries, CV spectra of Zn//Cu half cells, AFM imaging, changes in the flatness, grazing-incidence XRD patterns of the pole pieces of the Zn−Zn+GF/A symmetric battery, EIS curves of Zn/Zn symmetrical batteris with variable temperature, fitting curves of variable temperature EIS curves, distance versus binding energies, electrostatic surface potential of ACE-10 membrane on Zn^{2+}, chronoamperometry of the Zn/Zn symmetric batteries assembled, molar mass of each piece of ACE-10 membrane and the content of Zn^{2+} and SO_4^{2-} in it, Raman spectrum of $Zn(OTF)_2$, the combination form of carbonyl, ether and water in ACE-10 membrane molecule, computational simulation of the initial and final states of zinc hexahydrate near ACE-10 membrane, XRD patterns of ACC and ACC/I_2, SEM imaging and mapping of ACC/I_2, discharge curves of two batteries after 48 h of rest, rate performance of ACE-10 membrane assembled Zn/I_2 batteries, cycling performance of the zinc−iodine full batteries assembled at a current density of 1 C, cycling performance of the zinc−iodine full batteries assembled at a current density of 2 C, voltage-capacity plot of ACE-10 battery at a current density of 5 C, cycling performance of the zinc−iodine full batteries assembled with ACE-10 membrane at a current density of 5 C, solid surface zeta potential of ACE-10 membrane, *in situ* Raman curves of Zn-iodine batteries assembled with ACE-10 membrane and GF/A, flatness values for ACE-10 and GF/A diaphragms at different times of cycling, charge transfer resistance values for ACE-10 membrane and GF/A, binding energies by calculation and fitting, the comparison of electrochemical performance, the comparison of the strength of ACE-10 membrane with recently reported modified electrolytes (PDF)

Demonstration of the hexahydrated zinc ion close to the ACE-10 molecule (MP4)

H-type electrolytic cell with ACE-10 membrane in 2 h (MP4)

H-type electrolytic cell with GF/A in 2 h (MP4)

AUTHOR INFORMATION

Corresponding Authors

Yang Yang − *College of Chemistry and Chemical Engineering, State-Province Joint Engineering Laboratory of Power Source Technology for New Energy Vehicle, Tan Kah Kee Innovation Laboratory (IKKEM), State Key Laboratory of Physical Chemistry of Solid Surfaces, Xiamen University, Xiamen 361005, P. R. China*; orcid.org/0000-0003-4215-5767; Email: yangyang419@xmu.edu.cn

Jinbao Zhao − *College of Chemistry and Chemical Engineering, State-Province Joint Engineering Laboratory of Power Source Technology for New Energy Vehicle, Tan Kah Kee Innovation Laboratory (IKKEM), State Key Laboratory of Physical Chemistry of Solid Surfaces, Xiamen University, Xiamen 361005, P. R. China*; orcid.org/0000-0002-2753-7508; Email: jbzhao@xmu.edu.cn

Authors

Pengxiang Lin − *College of Chemistry and Chemical Engineering, State-Province Joint Engineering Laboratory of Power Source Technology for New Energy Vehicle, Tan Kah Kee Innovation Laboratory (IKKEM), State Key Laboratory of Physical Chemistry of Solid Surfaces, Xiamen University, Xiamen 361005, P. R. China*

Guanhong Chen − *College of Chemistry and Chemical Engineering, State-Province Joint Engineering Laboratory of Power Source Technology for New Energy Vehicle, Tan Kah Kee Innovation Laboratory (IKKEM), State Key Laboratory of Physical Chemistry of Solid Surfaces, Xiamen University, Xiamen 361005, P. R. China*

Yuanhong Kang − *College of Chemistry and Chemical Engineering, State-Province Joint Engineering Laboratory of Power Source Technology for New Energy Vehicle, Tan Kah Kee Innovation Laboratory (IKKEM), State Key Laboratory of Physical Chemistry of Solid Surfaces, Xiamen University, Xiamen 361005, P. R. China*

https://doi.org/10.1021/acsnano.3c01518
ACS Nano 2023, 17, 15492−15503

Minghao Zhang − *College of Chemistry and Chemical Engineering, State-Province Joint Engineering Laboratory of Power Source Technology for New Energy Vehicle, Tan Kah Kee Innovation Laboratory (IKKEM), State Key Laboratory of Physical Chemistry of Solid Surfaces, Xiamen University, Xiamen 361005, P. R. China*

Jin Yang − *College of Chemistry and Chemical Engineering, State-Province Joint Engineering Laboratory of Power Source Technology for New Energy Vehicle, Tan Kah Kee Innovation Laboratory (IKKEM), State Key Laboratory of Physical Chemistry of Solid Surfaces, Xiamen University, Xiamen 361005, P. R. China*

Zeheng Lv − *College of Chemistry and Chemical Engineering, State-Province Joint Engineering Laboratory of Power Source Technology for New Energy Vehicle, Tan Kah Kee Innovation Laboratory (IKKEM), State Key Laboratory of Physical Chemistry of Solid Surfaces, Xiamen University, Xiamen 361005, P. R. China*

Complete contact information is available at: https://pubs.acs.org/10.1021/acsnano.3c01518

Author Contributions

Pengxiang Lin: Conceptualization, Methodology, Investigation, Software, Writing−original draft. Guanhong Chen: Investigation, Formal analysis. Yuanhong Kang: Formal analysis. Minghao Zhang: Formal analysis. Jin Yang: Validation. Zeheng Lv: Supervision. Yang Yang: Supervision, Writing−review and editing, Project administration. Jinbao Zhao: Supervision, Writing−review and editing, Funding acquisition.

Notes

The authors declare no competing financial interest.

ACKNOWLEDGMENTS

This work is supported by National Natural Science Foundation of China (22109030 and 22021001), Fundamental Research Funds for the Central Universities (20720220073), Key R&D Program of Yunnan Province (No. 202103AA080019), Fujian Industrial Technology Development and Application Plan (2022I0002), and Guangdong Province Basic and Applied Basic Research Fund (2021A1515010177). We are grateful to the Tan Kah Kee Innovation Laboratory (IKKEM) for help with ICP and Raman tests. Numerical computations were performed at the Hefei advanced computing center.

REFERENCES

(1) Xie, C.; Li, T.; Deng, C.; Song, Y.; Zhang, H.; Li, X. A highly reversible neutral zinc/manganese battery for stationary energy storage. *Energy Environ. Sci.* **2020**, *13*, 135−143.

(2) Zhao, W. China's goal of achieving carbon neutrality before 2060: experts explain how. *Natl. Sci. Rev.* **2022**, *9*, nwac115.

(3) Hao-miao, L.; Hao, Z.; Kang-li, W.; Kai, J. Liquid Metal Electrodes for Electrochemical Energy Storage Technologies. *J. Electrochem.* **2020**, *26*, 663.

(4) Liu, S.; Zhang, R.; Mao, J.; Zhao, Y.; Cai, Q.; Guo, Z. From room temperature to harsh temperature applications: Fundamentals and perspectives on electrolytes in zinc metal batteries. *Sci. Adv.* **2022**, *8*, No. eabn5097.

(5) Zhang, L.; Hou, Y. Comprehensive analyses of aqueous Zn metal batteries: characterization methods, simulations, and theoretical calculations. *Adv. Energy Mater.* **2021**, *11*, 2003823.

(6) Wu, K.; Huang, J.; Yi, J.; Liu, X.; Liu, Y.; Wang, Y.; Zhang, J.; Xia, Y. Recent advances in polymer electrolytes for zinc ion batteries: mechanisms, properties, and perspectives. *Adv. Energy Mater.* **2020**, *10*, 1903977.

(7) Wang, X.; Zhang, Z.; Xi, B.; Chen, W.; Jia, Y.; Feng, J.; Xiong, S. Advances and perspectives of cathode storage chemistry in aqueous zinc-ion batteries. *ACS Nano* **2021**, *15*, 9244−9272.

(8) Xie, C.; Li, Y.; Wang, Q.; Sun, D.; Tang, Y.; Wang, H. Issues and solutions toward zinc anode in aqueous zinc-ion batteries: A mini review. *Carbon Energy* **2020**, *2*, 540−560.

(9) Lv, Y.; Xiao, Y.; Ma, L.; Zhi, C.; Chen, S. Recent Advances in Electrolytes for "Beyond Aqueous" Zinc-Ion Batteries. *Adv. Mater.* **2022**, *34*, 2106409.

(10) Pan, H.; Shao, Y.; Yan, P.; Cheng, Y.; Han, K. S.; Nie, Z.; Wang, C.; Yang, J.; Li, X.; Bhattacharya, P.; Mueller, K. T.; Liu, J. Reversible aqueous zinc/manganese oxide energy storage from conversion reactions. *Nat. Energy* **2016**, *1*, 1−7.

(11) Javed, M. S.; Asim, S.; Najam, T.; Khalid, M.; Hussain, I.; Ahmad, A.; Assiri, M. A.; Han, W. Recent progress in flexible Zn-ion hybrid supercapacitors: Fundamentals, fabrication designs, and applications. *Carbon Energy* **2023**, *5*, No. e271.

(12) Ren, Y.; Meng, F.; Zhang, S.; Ping, B.; Li, H.; Yin, B.; Ma, T. CNT@ MnO2 composite ink toward a flexible 3D printed micro-zinc-ion battery. *Carbon Energy* **2022**, *4*, 446−457.

(13) Li, W.; Han, C.; Gu, Q.; Chou, S. L.; Wang, J. Z.; Liu, H. K.; Dou, S. X. Electron Delocalization and Dissolution-Restraint in Vanadium Oxide Superlattices to Boost Electrochemical Performance of Aqueous Zinc-Ion Batteries. *Adv. Energy Mater.* **2020**, *10*, 2001852.

(14) Liu, S.; Zhu, H.; Zhang, B.; Li, G.; Zhu, H.; Ren, Y.; Geng, H.; Yang, Y.; Liu, Q.; Li, C. C. Tuning the kinetics of zinc-ion insertion/extraction in V2O5 by in situ polyaniline intercalation enables improved aqueous zinc-ion storage performance. *Adv. Mater.* **2020**, *32*, 2001113.

(15) Ma, L.; Chen, S.; Long, C.; Li, X.; Zhao, Y.; Liu, Z.; Huang, Z.; Dong, B.; Zapien, J. A.; Zhi, C. Achieving high-voltage and high-capacity aqueous rechargeable zinc ion battery by incorporating two-species redox reaction. *Adv. Energy Mater.* **2019**, *9*, 1902446.

(16) Zhang, J.; Lei, Q.; Ren, Z.; Zhu, X.; Li, J.; Li, Z.; Liu, S.; Ding, Y.; Jiang, Z.; Li, J.; Huang, Y.; Li, X.; Zhou, X.; Wang, Y.; Zhu, D.; Zeng, M.; Fu, L. A superlattice-stabilized layered CuS anode for high-performance aqueous zinc-ion batteries. *ACS Nano* **2021**, *15*, 17748−17756.

(17) Blanc, L. E.; Kundu, D.; Nazar, L. F. Scientific challenges for the implementation of Zn-ion batteries. *Joule* **2020**, *4*, 771−799.

(18) Yang, Y.; Liang, S.; Lu, B.; Zhou, J. Eutectic electrolyte based on N-methylacetamide for highly reversible zinc−iodine battery. *Energy Environ. Sci.* **2022**, *15*, 1192−1200.

(19) Zhao, D.; Zhu, Q.; Zhou, Q.; Zhang, W.; Yu, Y.; Chen, S.; Ren, Z. Enhancing I0/I-conversion efficiency by starch confinement in zinc−iodine battery. *Energy Environ. Mater.* **2023**, No. e12522.

(20) Ma, J.; Liu, M.; He, Y.; Zhang, J. Iodine redox chemistry in rechargeable batteries. *Angew. Chem., Int. Ed.* **2021**, *60*, 12636−12647.

(21) Yan, L.; Zhang, S.; Kang, Q.; Meng, X.; Li, Z.; Liu, T.; Ma, T.; Lin, Z. Iodine Conversion Chemistry in Aqueous Batteries: Challenges, Strategies, and Perspectives. *Energy Storage Mater.* **2023**, *54*, 339−365.

(22) Pan, H.; Li, B.; Mei, D.; Nie, Z.; Shao, Y.; Li, G.; Li, X. S.; Han, K. S.; Mueller, K. T.; Sprenkle, V.; Liu, J. Controlling solid−liquid conversion reactions for a highly reversible aqueous zinc−iodine battery. *ACS Energy Lett.* **2017**, *2*, 2674−2680.

(23) Zhang, Y.; Zheng, X.; Wu, K.; Zhang, Y.; Xu, G.; Wu, M.; Liu, H.-K.; Dou, S.-X.; Wu, C. Nonionic Surfactant-Assisted In Situ Generation of Stable Passivation Protective Layer for Highly Stable Aqueous Zn Metal Anodes. *Nano Lett.* **2022**, *22*, 8574−8583.

(24) Zhao, M.; Lv, Y.; Zhao, S.; Xiao, Y.; Niu, J.; Yang, Q.; Qiu, J.; Wang, F.; Chen, S. Simultaneously Stabilizing both Electrodes and Electrolytes by a Self-Separating Organometallics Interface for High Performance Zinc-Ion Battery at Wide Temperatures. *Adv. Mater.* **2022**, *34*, 2206239.

(25) Yang, H.; Qiao, Y.; Chang, Z.; Deng, H.; He, P.; Zhou, H. A Metal−Organic Framework as a Multifunctional Ionic Sieve

Membrane for Long-Life Aqueous Zinc−Iodide Batteries. *Adv. Mater.* **2020**, *32*, 2004240.
(26) Ito, S.; Sugimasa, M.; Toshimitsu, Y.; Orita, A.; Kitagawa, M.; Sakai, M. Formation of a hydrophobic polyiodide complex during cathodic oxidation of iodide in the presence of propylene carbonate in aqueous solutions, and its application to a zinc/iodine redox flow battery. *Electrochim. Acta* **2019**, *319*, 164−174.
(27) Qin, R.; Wang, Y.; Yao, L.; Yang, L.; Zhao, Q.; Ding, S.; Liu, L.; Pan, F. Progress in interface structure and modification of zinc anode for aqueous batteries. *Nano Energy* **2022**, *98*, 107333.
(28) Han, D.; Wu, S.; Zhang, S.; Deng, Y.; Cui, C.; Zhang, L.; Long, Y.; Li, H.; Tao, Y.; Weng, Z.; Yang, Q.-H.; Kang, F. A corrosion-resistant and dendrite-free zinc metal anode in aqueous systems. *Small* **2020**, *16*, 2001736.
(29) Wang, P.; Liang, S.; Chen, C.; Xie, X.; Chen, J.; Liu, Z.; Tang, Y.; Lu, B.; Zhou, J. Spontaneous Construction of Nucleophilic Carbonyl-Containing Interphase toward Ultrastable Zinc-Metal Anodes. *Adv. Mater.* **2022**, *34*, 2202733.
(30) Li, Q.; Chen, A.; Wang, D.; Zhao, Y.; Wang, X.; Jin, X.; Xiong, B.; Zhi, C. Tailoring the metal electrode morphology via electrochemical protocol optimization for long-lasting aqueous zinc batteries. *Nat. Commun.* **2022**, *13*, 1−9.
(31) Tian, Y.; An, Y.; Wei, C.; Xi, B.; Xiong, S.; Feng, J.; Qian, Y. Flexible and free-standing Ti3C2T x MXene@ Zn paper for dendrite-free aqueous zinc metal batteries and nonaqueous lithium metal batteries. *ACS Nano* **2019**, *13*, 11676−11685.
(32) He, X.; Cui, Y.; Qian, Y.; Wu, Y.; Ling, H.; Zhang, H.; Kong, X.-Y.; Zhao, Y.; Xue, M.; Jiang, L.; Wen, L. Anion Concentration Gradient-Assisted Construction of a Solid−Electrolyte Interphase for a Stable Zinc Metal Anode at High Rates. *J. Am. Chem. Soc.* **2022**, *144*, 11168−11177.
(33) Bai, C.; Cai, F.; Wang, L.; Guo, S.; Liu, X.; Yuan, Z. A sustainable aqueous Zn-I2 battery. *Nano Res.* **2018**, *11*, 3548−3554.
(34) Wu, W.; Li, C.; Wang, Z.; Shi, H.-Y.; Song, Y.; Liu, X.-X.; Sun, X. Electrode and electrolyte regulation to promote coulombic efficiency and cycling stability of aqueous zinc-iodine batteries. *Chem. Eng. J.* **2022**, *428*, 131283.
(35) Zeng, X.; Meng, X.; Jiang, W.; Liu, J.; Ling, M.; Yan, L.; Liang, C. Anchoring polyiodide to conductive polymers as cathode for high-performance aqueous zinc−iodine batteries. *ACS Sustainable Chem. Eng.* **2020**, *8*, 14280−14285.
(36) Wang, F.; Liu, Z.; Yang, C.; Zhong, H.; Nam, G.; Zhang, P.; Dong, R.; Wu, Y.; Cho, J.; Zhang, J.; Feng, X. Fully Conjugated Phthalocyanine Copper Metal−Organic Frameworks for Sodium−Iodine Batteries with Long-Time-Cycling Durability. *Adv. Mater.* **2020**, *32*, 1905361.
(37) Kundu, D.; Hosseini Vajargah, S.; Wan, L.; Adams, B.; Prendergast, D.; Nazar, L. F. Aqueous vs. nonaqueous Zn-ion batteries: consequences of the desolvation penalty at the interface. *Energy Environ. Sci.* **2018**, *11*, 881−892.
(38) Zhou, L.-F.; Du, T.; Li, J.-Y.; Wang, Y.; Gong, H.; Yang, Q.-R.; Chen, H.; Luo, W.; Wang, J. A strategy for anode modification for future zinc-based battery application. *Mater. Horiz.* **2022**, *9*, 2722−2751.
(39) Chen, S.; Nian, Q.; Zheng, L.; Xiong, B.-Q.; Wang, Z.; Shen, Y.; Ren, X. Highly reversible aqueous zinc metal batteries enabled by fluorinated interphases in localized high concentration electrolytes. *J. Mater. Chem. A* **2021**, *9*, 22347−22352.
(40) Zou, Y.; Liu, T.; Du, Q.; Li, Y.; Yi, H.; Zhou, X.; Li, Z.; Gao, L.; Zhang, L.; Liang, X. A four-electron Zn-I2 aqueous battery enabled by reversible I−/I2/I+ conversion. *Nat. Commun.* **2021**, *12*, 1−11.
(41) Yang, W.; Du, X.; Zhao, J.; Chen, Z.; Li, J.; Xie, J.; Zhang, Y.; Cui, Z.; Kong, Q.; Zhao, Z.; Wang, C.; Zhang, Q.; Cui, G. Hydrated eutectic electrolytes with ligand-oriented solvation shells for long-cycling zinc-organic batteries. *Joule* **2020**, *4*, 1557−1574.
(42) Miao, L.; Wang, R.; Di, S.; Qian, Z.; Zhang, L.; Xin, W.; Liu, M.; Zhu, Z.; Chu, S.; Du, Y.; Zhang, N. Aqueous Electrolytes with Hydrophobic Organic Cosolvents for Stabilizing Zinc Metal Anodes. *ACS Nano* **2022**, *16*, 9667−9678.
(43) Zhang, S. J.; Hao, J.; Li, H.; Zhang, P. F.; Yin, Z. W.; Li, Y. Y.; Zhang, B.; Lin, Z.; Qiao, S. Z. Polyiodide Confinement by Starch Enables Shuttle-Free Zn−Iodine Batteries. *Adv. Mater.* **2022**, *34*, 2201716.
(44) Zhang, X.; Li, J.; Qi, K.; Yang, Y.; Liu, D.; Wang, T.; Liang, S.; Lu, B.; Zhu, Y.; Zhou, J. An Ion-Sieving Janus Separator toward Planar Electrodeposition for Deeply Rechargeable Zn-Metal Anodes. *Adv. Mater.* **2022**, *34*, 2205175.
(45) Zhang, P.-F.; Wu, Z.; Zhang, S.-J.; Liu, L.-Y.; Tian, Y.; Dou, Y.; Lin, Z.; Zhang, S. Tannin acid induced anticorrosive film toward stable Zn-ion batteries. *Nano Energy* **2022**, *102*, 107721.
(46) Fan, H.; Wang, M.; Yin, Y.; Liu, Q.; Tang, B.; Sun, G.; Wang, E.; Li, X. Tailoring interfacial Zn2+ coordination via a robust cation conductive film enables high performance zinc metal battery. *Energy Storage Mater.* **2022**, *49*, 380−389.
(47) Zhang, X.; Li, J.; Qi, K.; Yang, Y.; Liu, D.; Wang, T.; Liang, S.; Lu, B.; Zhu, Y.; Zhou, J. An Ion-Sieving Janus Separator toward Planar Electrodeposition for Deeply Rechargeable Zn-Metal Anodes. *Adv. Mater.* **2022**, *34*, 2205175.
(48) Zhang, Y.; Yang, G.; Lehmann, M. L.; Wu, C.; Zhao, L.; Saito, T.; Liang, Y.; Nanda, J.; Yao, Y. Separator effect on zinc electrodeposition behavior and its implication for zinc battery lifetime. *Nano Lett.* **2021**, *21*, 10446−10452.
(49) Liang, Y.; Ma, D.; Zhao, N.; Wang, Y.; Yang, M.; Ruan, J.; Yang, G.; Mi, H.; He, C.; Zhang, P. Novel Concept of Separator Design: Efficient Ions Transport Modulator Enabled by Dual-Interface Engineering Toward Ultra-Stable Zn Metal Anodes. *Adv. Funct. Mater.* **2022**, *32*, 2112936.
(50) Li, Z.; Wu, X.; Yu, X.; Zhou, S.; Qiao, Y.; Zhou, H.; Sun, S.-G. Long-Life Aqueous Zn−I2 Battery Enabled by a Low-Cost Multifunctional Zeolite Membrane Separator. *Nano Lett.* **2022**, *22*, 2538−2546.
(51) Hou, Y.; Kong, F.; Wang, Z.; Ren, M.; Qiao, C.; Liu, W.; Yao, J.; Zhang, C.; Zhao, H. High performance rechargeable aqueous zinc-iodine batteries via a double iodine species fixation strategy with mesoporous carbon and modified separator. *J. Colloid Interface Sci.* **2023**, *629*, 279−287.
(52) Bai, C.; Jin, H.; Gong, Z.; Liu, X.; Yuan, Z. A high-power aqueous rechargeable Fe-I2 battery. *Energy Storage Mater.* **2020**, *28*, 247−254.
(53) Huang, B.; Hua, H.; Lai, P.; Shen, X.; Li, R.; He, Z.; Zhang, P.; Zhao, J. Constructing Ion-Selective Coating Layer with Lithium Ion Conductor LLZO and Binder Li-Nafion for Separator Used in Lithium-Sulfur Batteries. *ChemElectroChem.* **2022**, *9*, No. e202200416.
(54) Sachan, S.; Ray, C. A.; Perusich, S. A. Lithium ion transport through nonaqueous perfluoroionomeric membranes. *Polym. Eng. Sci.* **2002**, *42*, 1469−1480.
(55) Bauer, I.; Thieme, S.; Brückner, J.; Althues, H.; Kaskel, S. Reduced polysulfide shuttle in lithium−sulfur batteries using Nafion-based separators. *J. Power Sources* **2014**, *251*, 417−422.
(56) Zhou, W.; Chen, M.; Tian, Q.; Chen, J.; Xu, X.; Wong, C.-P. Cotton-derived cellulose film as a dendrite-inhibiting separator to stabilize the zinc metal anode of aqueous zinc ion batteries. *Energy Storage Mater.* **2022**, *44*, 57−65.
(57) Wu, M.; Zhang, Y.; Xu, L.; Yang, C.; Hong, M.; Cui, M.; Clifford, B. C.; He, S.; Jing, S.; Yao, Y.; Hu, L. A sustainable chitosan-zinc electrolyte for high-rate zinc-metal batteries. *Matter* **2022**, *5*, 3402−3416.
(58) Fang, Y.; Xie, X.; Zhang, B.; Chai, Y.; Lu, B.; Liu, M.; Zhou, J.; Liang, S. Regulating zinc deposition behaviors by the conditioner of PAN separator for zinc-ion batteries. *Adv. Funct. Mater.* **2022**, *32*, 2109671.
(59) Wu, B.; Wu, Y.; Lu, Z.; Zhang, J.; Han, N.; Wang, Y.; Li, X.-m.; Lin, M.; Zeng, L. A cation selective separator induced cathode protective layer and regulated zinc deposition for zinc ion batteries. *J. Mater. Chem. A* **2021**, *9*, 4734−4743.
(60) Xu, L.; Meng, T.; Zheng, X.; Li, T.; Brozena, A. H.; Mao, Y.; Zhang, Q.; Clifford, B. C.; Rao, J.; Hu, L. Nanocellulose-

https://doi.org/10.1021/acsnano.3c01518
ACS Nano 2023, 17, 15492−15503

Carboxymethylcellulose Electrolyte for Stable, High-Rate Zinc-Ion Batteries. *Adv. Funct. Mater.* **2023**, *33*, 2302098.
(61) Zhang, H.; Gan, X.; Song, Z.; Zhou, J. Amphoteric Cellulose-Based Double-Network Hydrogel Electrolyte Toward Ultra-Stable Zn Anode. *Angew. Chem.* **2023**, *135*, No. e202217833.
(62) Yan, Y.; Duan, S.; Liu, B.; Wu, S.; Alsaid, Y.; Yao, B.; Nandi, S.; Du, Y.; Wang, T.-W.; Li, Y.; He, X. Tough Hydrogel Electrolytes for Anti-Freezing Zinc-Ion Batteries. *Adv. Mater.* **2023**, *35*, 2211673.
(63) Li, M.; Xi, C.; Wang, X.; Li, L.; Xiao, Y.; Chao, Y.; Zheng, X.; Liu, Z.; Yu, Y.; Yang, C. Spontaneous Desaturation of the Solvation Sheath for High-Performance Anti-Freezing Zinc-Ion Gel-Electrolyte. *Small* **2023**, 2301569.
(64) Lin, P.; Cong, J.; Li, J.; Zhang, M.; Lai, P.; Zeng, J.; Yang, Y.; Zhao, J. Achieving ultra-long lifespan Zn metal anodes by manipulating desolvation effect and Zn deposition orientation in a multiple cross-linked hydrogel electrolyte. *Energy Storage Mater.* **2022**, *49*, 172−180.
(65) Yang, F.; Hua, H.; Lai, P.; Lin, P.; Yang, J.; Zhang, M.; Yang, Y.; Zhao, J. Synergetic Modulation of Ion Flux and Water Activity in a Single Zn2+ Conductor Hydrogel Electrolyte for Ultrastable Aqueous Zinc-Ion Batteries. *ACS Appl. Energy Mater.* **2022**, *5*, 10872−10882.
(66) Wu, F.; Du, F.; Ruan, P.; Cai, G.; Chen, Y.; Yin, X.; Ma, L.; Yin, R.; Shi, W.; Liu, W.; Zhou, J.; Cao, X. Regulating zinc deposition behaviors by functional PANI modification layer on separator for high performance aqueous zinc-ion batteries. *J. Mater. Chem. A* **2023**, *11*, 11254.
(67) Yang, Y.; Liu, C.; Lv, Z.; Yang, H.; Zhang, Y.; Ye, M.; Chen, L.; Zhao, J.; Li, C. C. Synergistic manipulation of Zn2+ ion flux and desolvation effect enabled by anodic growth of a 3D ZnF2 matrix for long-lifespan and dendrite-free Zn metal anodes. *Adv. Mater.* **2021**, *33*, 2007388.
(68) Kim, J. Y.; Liu, G.; Shim, G. Y.; Kim, H.; Lee, J. K. Functionalized Zn@ ZnO hexagonal pyramid array for dendrite-free and ultrastable zinc metal anodes. *Adv. Funct. Mater.* **2020**, *30*, 2004210.
(69) Yang, Y.; Liu, C.; Lv, Z.; Yang, H.; Cheng, X.; Zhang, S.; Ye, M.; Zhang, Y.; Chen, L.; Zhao, J.; Li, C. C. Redistributing Zn-ion flux by interlayer ion channels in Mg-Al layered double hydroxide-based artificial solid electrolyte interface for ultra-stable and dendrite-free Zn metal anodes. *Energy Storage Mater.* **2021**, *41*, 230−239.
(70) Nilsson, A.; Pettersson, L. G. The structural origin of anomalous properties of liquid water. *Nat. Commun.* **2015**, *6*, 1−11.
(71) Athokpam, B.; Ramesh, S. G.; McKenzie, R. H. Effect of hydrogen bonding on the infrared absorption intensity of OH stretch vibrations. *Chem. Phys.* **2017**, *488*, 43−54.
(72) Pietzsch, A.; Hennies, F.; Miedema, P. S.; Kennedy, B.; Schlappa, J.; Schmitt, T.; Strocov, V. N.; Föhlisch, A. Snapshots of the fluctuating hydrogen bond network in liquid water on the sub-femtosecond timescale with vibrational resonant inelastic x-ray scattering. *Phys. Rev. Lett.* **2015**, *114*, 088302.
(73) Cui, Y.; Zhao, Q.; Wu, X.; Chen, X.; Yang, J.; Wang, Y.; Qin, R.; Ding, S.; Song, Y.; Wu, J.; Yang, K.; Wang, Z.; Mei, Z.; Song, Z.; Wu, H.; Jiang, Z.; Qian, G.; Yang, L.; Pan, F. An interface-bridged organic−inorganic layer that suppresses dendrite formation and side reactions for ultra-long-life aqueous zinc metal anodes. *Angew. Chem., Int. Ed.* **2020**, *132*, 16737−16744.
(74) Xie, C.; Liu, Y.; Lu, W.; Zhang, H.; Li, X. Highly stable zinc−iodine single flow batteries with super high energy density for stationary energy storage. *Energy Environ. Sci.* **2019**, *12*, 1834−1839.
(75) Zhang, Y.; Zhao, T.; Yang, S.; Zhang, Y.; Ma, Y.; Wang, Z. Flexible PEDOT: PSS nanopapers as "anion-cation regulation" synergistic interlayers enabling ultra-stable aqueous zinc-iodine batteries. *J. Energy Chem.* **2022**, *75*, 310−320.
(76) Shang, W.; Li, Q.; Jiang, F.; Huang, B.; Song, J.; Yun, S.; Liu, X.; Kimura, H.; Liu, J.; Kang, L. Boosting Znǁ I2 Battery's Performance by Coating a Zeolite-Based Cation-Exchange Protecting Layer. *Nano-Micro Lett.* **2022**, *14*, 1−13.
(77) Dang, H. X.; Sellathurai, A. J.; Barz, D. P. An ion exchange membrane-free, ultrastable zinc-iodine battery enabled by functionalized graphene electrodes. *Energy Storage Mater.* **2023**, *55*, 680−690.
(78) Shang, W.; Zhu, J.; Liu, Y.; Kang, L.; Liu, S.; Huang, B.; Song, J.; Li, X.; Jiang, F.; Du, W.; Gao, Y.; Luo, H. Establishing high-performance quasi-solid Zn/I2 batteries with alginate-based hydrogel electrolytes. *ACS Appl. Mater. Interfaces* **2021**, *13*, 24756−24764.
(79) Su, Y.; Liu, B.; Zhang, Q.; Peng, J.; Wei, C.; Li, S.; Li, W.; Xue, Z.; Yang, X.; Sun, J. Printing-Scalable Ti3C2Tx MXene-Decorated Janus Separator with Expedited Zn2+ Flux toward Stabilized Zn Anodes. *Adv. Funct. Mater.* **2022**, *32*, 2204306.
(80) Chai, L.; Wang, X.; Hu, Y.; Li, X.; Huang, S.; Pan, J.; Qian, J.; Sun, X. In-MOF-Derived Hierarchically Hollow Carbon Nanostraws for Advanced Zinc-Iodine Batteries. *Adv. Sci.* **2022**, *9*, 2105063.
(81) Tian, Y.; Chen, S.; Ding, S.; Chen, Q.; Zhang, J. A highly conductive gel electrolyte with favorable ion transfer channels for long-lived zinc−iodine batteries. *Chem. Sci.* **2023**, *14*, 331−337.
(82) Xi, J.; Li, Z.; Yu, L.; Yin, B.; Wang, L.; Liu, L.; Qiu, X.; Chen, L. Effect of degree of sulfonation and casting solvent on sulfonated poly (ether ether ketone) membrane for vanadium redox flow battery. *J. Power Sources* **2015**, *285*, 195−204.
(83) Xin, L.; Zhang, D.; Qu, K.; Lu, Y.; Wang, Y.; Huang, K.; Wang, Z.; Jin, W.; Xu, Z. Zr-MOF-Enabled Controllable Ion Sieving and Proton Conductivity in Flow Battery Membrane. *Adv. Funct. Mater.* **2021**, *31*, 2104629.
(84) Wang, Y.; Sun, Q.; Zhao, Q.; Cao, J.; Ye, S. Rechargeable lithium/iodine battery with superior high-rate capability by using iodine−carbon composite as cathode. *Energy Environ. Sci.* **2011**, *4*, 3947−3950.
(85) Tian, H.; Gao, T.; Li, X.; Wang, X.; Luo, C.; Fan, X.; Yang, C.; Suo, L.; Ma, Z.; Han, W.; Wang, C. High power rechargeable magnesium/iodine battery chemistry. *Nat. Commun.* **2017**, *8*, 1−8.

https://doi.org/10.1021/acsnano.3c01518
ACS Nano 2023, 17, 15492−15503